Perching and Vertical Climbing: Design of a Multimodal Robot

Matthew A. Estrada, Elliot W. Hawkes, David L. Christensen, Mark R. Cutkosky

***Abstract*— We present a robot capable of both (1) dynamically perching onto smooth, flat surfaces from a ballistic trajectory and (2) successfully transitioning to a climbing gait. Merging these two modes of movement is achieved via a mechanism utilizing an opposed grip with directional adhesives. Critical design considerations include (a) climbing mechanism weight constraints, (b) suitable body geometry for climbing and (c) effects of impact dynamics. The robot uses a symmetric linkage and cam mechanism to load and detach the feet while climbing. The lengths of key parameters, including the distances between each the feet and the tail, are chosen based on the ratio of required preload force and detachment force for the adhesive mechanism.**

I. Introduction

Over the past decade, mobile robots have become increasingly multimodal to extend their versatility in unstructured environments. Examples include the DALER robot [1], the Hybrid terrestrial and Aerial Quadrotor (HyTAQ) [2] and the biomimetic (BOLT) [3], which can all traverse both ground and air. Similarly, the STRIDe lab's robotic platform transitions from climbing to gliding [4] and Scout combines ballistic trajectories with crawling [5]. A complimentary next step to broaden robotic locomotion is to enable transitioning from aerial to scansorial motion.

The ability to perch and crawl on vertical surfaces offers a host of applications as a standalone platform and a way to extend the capabilities of aerial platforms. Climbing robots capable of perching could be thrown over obstacles to reach target surfaces or launched to higher starting points to avoid the need to carry the onboard energy required to scale long distances. Additionally, the ability to relocate the robot upon a wall compensates against any inaccuracy in launching. If kept lightweight and compact, the unit could be used as an addition to a platform capable of flight. For instance, a surveillance UAV could crawl along a wall if wind conditions or constrained spaces did not permit sustained flight. A robot capable of ballistic motion followed by gripping and crawling with adhesive could also be used to attach and service spacecraft. The presented work combines prior art to produce a system capable of both perching from free-flight and climbing on smooth vertical surfaces.

Several recent examples of perching robots have been demonstrated. However, they lack the ability to reposition themselves while on a surface. Perching is often accomplished with terrain-specific attachment mechanisms such as gecko-inspired adhesives for smooth surfaces [6,7], spines for rough surfaces [8], or bird-like feet for grasping wires or poles [9].

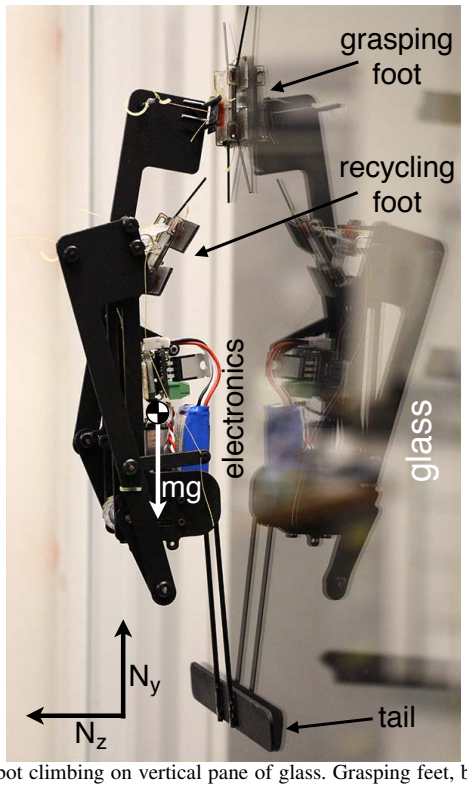

Fig. 1: Robot climbing on vertical pane of glass. Grasping feet, battery, and electronics can be see on the underside.

Vertical surface climbing has likewise received attention, employing mechanisms such as spines and adhesives for rough and smooth surfaces, respectively [10]–[12]. Waalbot adhered additionally to inverted surfaces [13,14] and CLASH achieved dynamic, near-vertical climbing [15].

Realizing functionality in both domains requires generating adhesion adequate for perching while maintaining low weight and sufficient articulation for climbing. These requirements are fulfilled by adapting a surface grasping mechanism recently described in [7] and creating a simple, symmetric climbing gait actuated by a single motor.

The directional adhesive used is made up of an array of angled, silicone wedges. These wedges generate adhesion when they are loaded tangentially and comply towards a surface [16]. Thus, the adhesion force is a function of the shear force being applied to the adhesive pad. The adhesive is able to conform to asperities on the order of the height of its wedges, about 100 microns, which makes its efficacy dependent upon the roughness, flatness and cleanliness of a surface as well.

The gripping mechanism uses two pads of directional

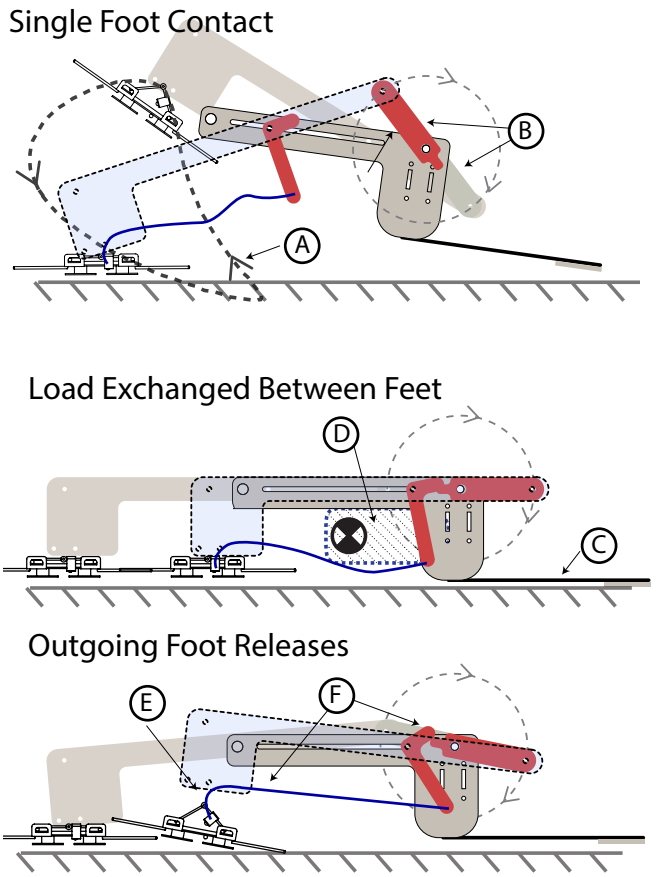

Fig. 2: Schematic depiction of components on robot. (A) Foot trajectory taken with respect to chassis frame (B) Legs offset 180 degrees out of phase within gait (C) Tail for robot (D) Location of motor, electronics and center of mass (E) Compliance at ankle-foot interface and (F) Cam trigger mechanism for foot release.

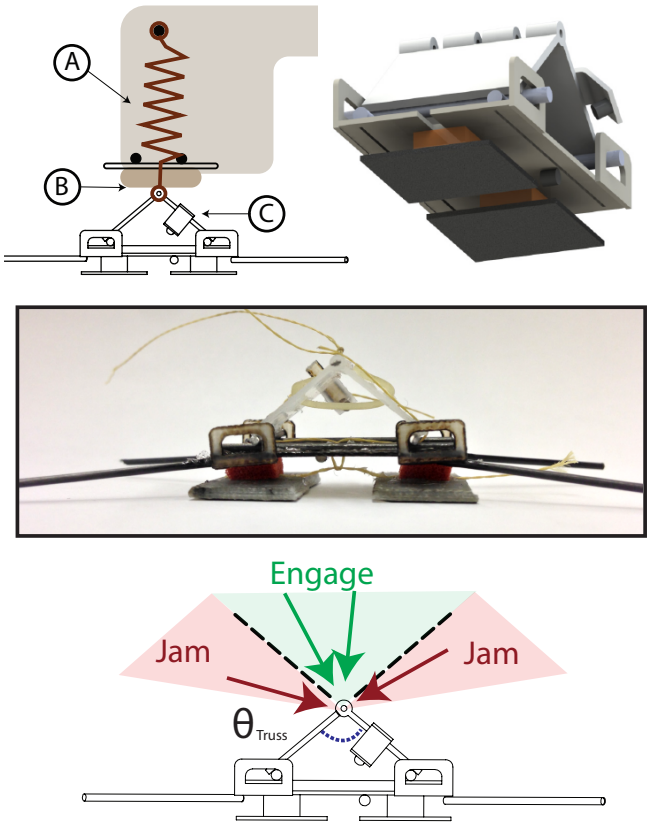

Fig. 3: Design of the dynamic grasping foot. (A) Rebound spring allows for protection against overloading adhesive (B) Foam bedding acts as a universal joint (C) Magnetic latch attached to living hinge locks adhesive in an engaged state. Shown below is a photo of the foot as well as a depiction of acceptable truss collapsing angles (shown in green).

adhesives arranged in an opposed grip, similar to the tactics employed by geckos and cockroaches while climbing [17]. The opposed grip is controllable and utilizes each pad's shear load to create an adhesion force with sufficient safety margin to withstand the rebound force resulting from robot-wall collisions at the end of a ballistic trajectory.

II. Design and Analysis

Perching and climbing are both more easily realizable for small, light robots. A challenge for a multi-modal robot is to accomplish both tasks with a minimum of hardware. The presented design features open-loop, single-actuator climbing coordinated by an onboard microcontroller and lithium polymer battery. The structure is made from lightweight Birch plywood along with a carbon fiber tail. The general specifications of the robot are listed in Table I.

A. Mass Distribution for Climbing

Mass distribution, particularly placement of the heaviest components (electronics and actuation), is important to minimize undesirable moments while climbing. The robot is symmetric about its sagittal plane, as seen in the right side of Fig. 4, to prevent moments about the $\hat{N}_z$ direction that could interfere with attachment during climbing. The center of mass is also well below the feet to reduce unwanted turning while climbing directly up a wall. Additionally, the heaviest components were positioned as close as possible to the wall (Fig. 4 left) to reduce the peeling moment about $\hat{N}_x$. Equation 1 expresses the peeling moment balance on the robot body, A. Parameter d_{foot} is the $\hat{N}_y$ distance between the bottom of the chassis and foot, d_{tail} the $\hat{N}_y$ distance between bottom of the chassis and tail, and d_{cm} the $\hat{N}_z$ distance of the center of mass from the wall.

$$\Sigma \vec{M}^{A/A_{tail}} \cdot \hat{N}_x = d_{cm} * m_{robot} * g - (d_{foot} + d_{tail})(\vec{F}_{adhesion} \cdot \hat{N}_z) = 0$$

$$\vec{F}_{adhesion} \cdot \hat{N}_z = \frac{d_{cm} * m_{robot} * g}{d_{foot} + d_{tail}}. \quad (1)$$

The force of gravity is counteracted by $\vec{F}_{adhesion} \cdot \hat{N}_z$, the magnitude of normal adhesion. Additionally, the tail length d_{tail} reduces the magnitude of the adhesion force required for static equilibrium.

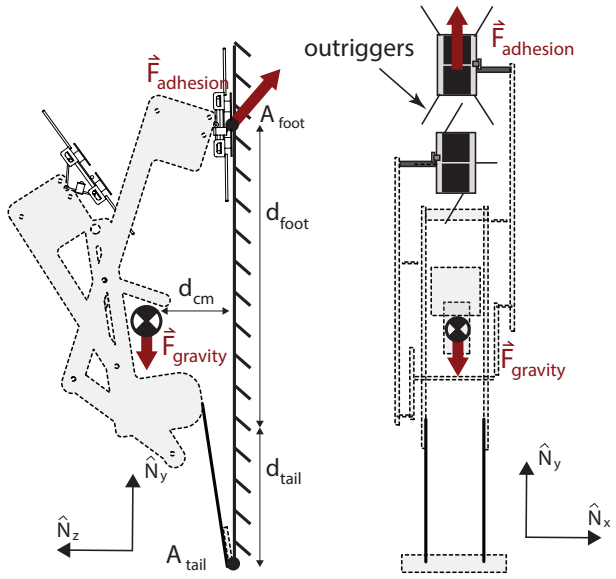

Fig. 4: Free body diagram of robot in a profile view showing peeling moment and underside view showing adhesive attachment inline with center of mass.

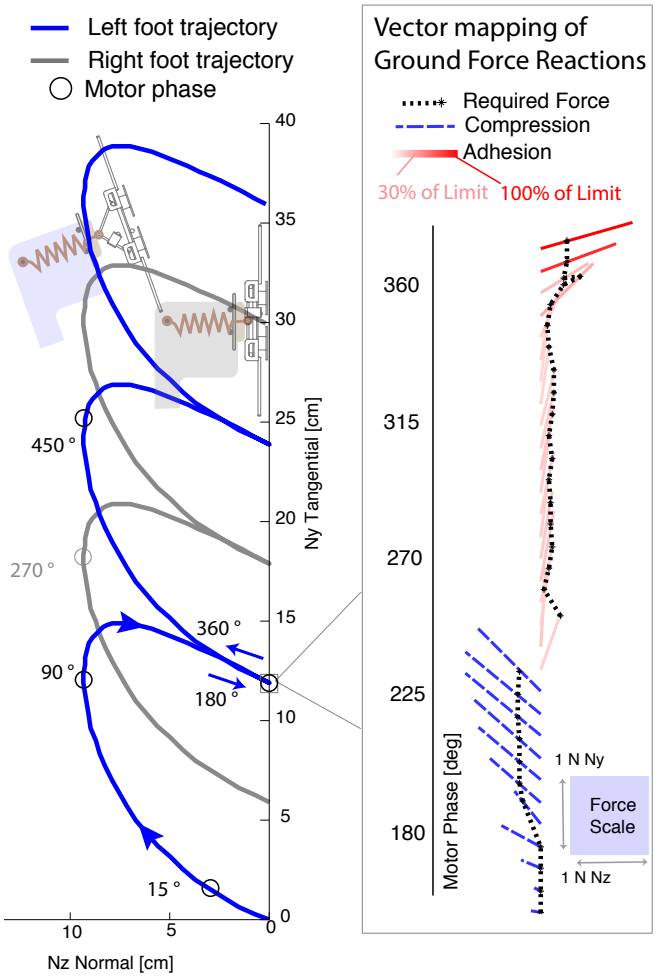

Fig. 5: Left: Foot trajectories up wall tagged with gait phase. Right: Force vectors experienced while foot is engaged with the wall, plotted according to gait phase.

B. Climbing Trajectory

Two parallel crank and pin-slider mechanisms give a cyclic crawling motion. The two feet operate 180 degrees out of phase, each following a trajectory labeled as A in Fig. 2. This trajectory allows the recycling foot to "leapfrog" the attached foot. A cam, labeled as F, triggers the release of a foot at the end of each step by pulling on a tendon, described further in Section II-C.

Keeping a small step size between the feet is advantageous to minimize the overall dimensions of the robot. To avoid collisions between the long "outriggers" (seen clearly in Fig. 3) that are used to align the feet to a surface, each is offset to nest with the other.

Each foot is engaged for a total of 190-200 degrees of gait cycle, measured in terms of the constant input crank velocity, indicated by B in Fig. 2. Compliance in the feet and ankles (labeled as E in the figure), allows both feet to remain attached while the load is being exchanged.

C. Interfacing with Dynamic Grasping Feet

The dynamic grasping feet are capable of engaging during impact and maintaining adhesion despite rebound forces. An additional advantage to this robust attachment method is the robot's decreased sensitivity to an imprecise climbing trajectory.

Each of the feet uses two, 1.6 cm^2 pads of directional adhesive fabricated from a lithographic mold [18]. On initial contact with the wall, outriggers push the under-constrained feet to ensure alignment with the surface before the adhesive pads make contact. A nonlinear rebound spring holds each foot onto the "ankle" (Fig. 3 A). The spring pulls the feet taut against a foam suspension (Fig. 3 B). At maximum extension, the tension in the spring is set slightly below the grasping foot's maximum force. As a result, loads capable of detaching the adhesives are only transferred after the rebound springs bottom out after 2.5 cm of travel. Transmitting forces through a tendon also mitigates the possibility of transferring moments to the adhesives [7].

An improvement from previous work is the inclusion of a magnetic latch that engages with a low 0.3 N force, and can support a maximum load greater than the 2.5 N adhesive limit. The latch is constructed from a plastic living hinge with a magnet attached at the end (Fig. 3 C). This hinged magnet is pulled into contact with its mating magnet as the gripping mechanism's triangular truss collapses. Once connected, the top magnet's body acts as a hard stop to keep gripper adhesives loaded in shear.

The feet are used in a cyclic manner through a release mechanism triggered by a cam (Fig. 2 F). The cam pulls a tendon that releases the magnetic latch, allowing the feet to detach. A return spring, embodied by the rubber band spanning the truss in the Fig. 3 photo, pulls the gripping truss mechanism back into its unloaded configuration.

TABLE I: Robot specifications

Specification	Measurement
Foot latching force	0.35 N
Latched foot, normal pull off force	2.5 N
Unlatched foot, normal pull off force	1 N
Total area of adhesive on each foot	3.4 cm^2
Robot weight	78 grams
Stride length	6 cm
Step frequency	0.25 Hz
Climbing speed	1.5 cm/s
Motor	Pololu Micro Metal Gearmotor
Battery	7.4 V 180 mAh, LiPo
Energy expended while climbing	40 J/m

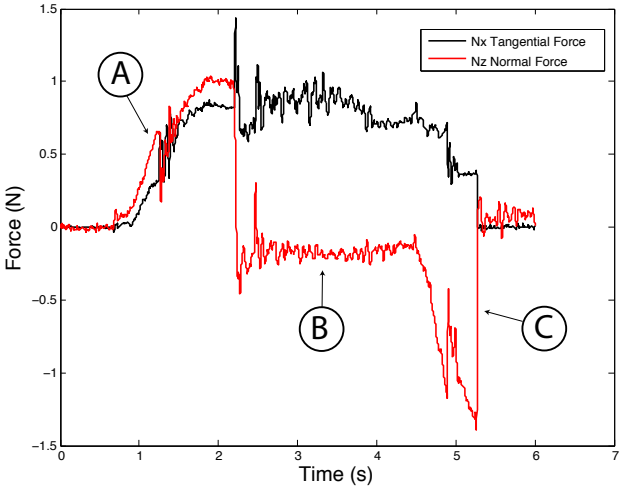

Fig. 6: Force profile acting on foot climbing vertically. Events shown are (A) Compression during foot engagement and detachment of outgoing foot (B) Pulling up the wall (C) Detachment of measured foot.

III. Experiments

An ATI-Gamma SI-32-2.5, six axis force/torque sensor (accuracy: +/- .05 N) measured dynamic forces at 1000 Hz during experiments. Sign conventions on measured forces follow those defined in Fig. 4.

A. Crawling Forces

1) Experimental Data: The experimental procedure had the robot step onto the force sensor with a single foot then continue through its gait until the measured foot released and detached. The data presented in Fig. 6 were passed through a zero-phase, third order Butterworth filter with cutoff frequency of 50 Hz.

A large normal force engages the incoming foot against the wall and continues to push to force the outgoing foot to separate from the wall in Fig. 6 A. The portion marked by Fig. 6 B is recognizable as the duration of the gait where only one foot is in contact with the wall. Finally, a tensile lift-off force is seen at 6 C, which serves to separate the foot from the wall. Until the feet unlatch, forces are within a safety factor of 2 from the adhesion limit. The largest force magnitudes experienced during crawling are in phases of engagement and detachment of the grasping feet.

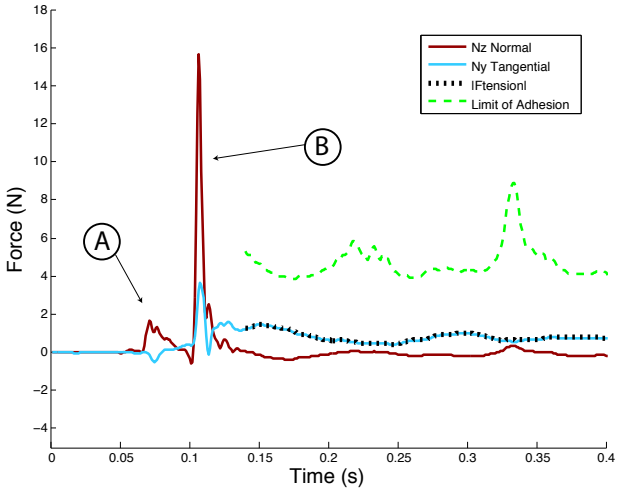

Fig. 7: Force profile of rebound forces felt at the foot latching onto glass with sensor mounted behind it. (A) indicates forces felt as the truss collapsed within the foot and (B) as the rigid structure of the robot came into contact.

2) Vector Mapping and Interpretation: Fig. 5 depicts the components of the reaction forces within Fig. 6 in a vector format. A force vector is drawn approximately every 7 degrees as the phase of the gait precesses. Intersecting each vector is a point indicating the magnitude of the "required force" necessary to hold the robot at static equilibrium in the particular configuration held during the gait. In the ideal case, all vectors would terminate at these black points. The vectors are also color coded to indicate compression (dashed blue) or tension (solid red). The red color intensity is proportional to the force magnitude as compared to the adhesion limit.

The two halves of Fig. 6 depict the intersection of foot trajectories and wall reaction forces. The left foot makes an arc through 0 - 180 degrees of the gait phase, clearing the right foot and attaching to the wall. Through the last half of the gait phase, 180-360 degrees, it experiences the progression of forces as depicted by the force vector mapping. At 360 degrees, it detaches and continues through another cycle.

It is apparent that the theoretical force necessary to climb is close to the measured force for the duration that one foot is in contact (for phase approximately 250-350 degrees). The black, dotted line is very close to the drawn vector magnitudes. However, longer force vectors at the beginning and end of foot contact make it apparent that comparatively large forces are required to detach the adhesive.

B. Landing Forces

In order to record landing forces during perching, the robot was launched at a glass plate mounted to the ATI sensor. The sensor measures only collision forces for the foot; tail impact occurred upon a surface in plane with the glass but isolated from the sensor. Landing forces are plotted in Fig. 7 with the resulting tensile force experienced at the rebound spring at the ankle. The force $F_{tension}$ was computed by calculating the magnitude of the force vector in the Y-Z plane for the duration that the foot was not in compression. The adhesion

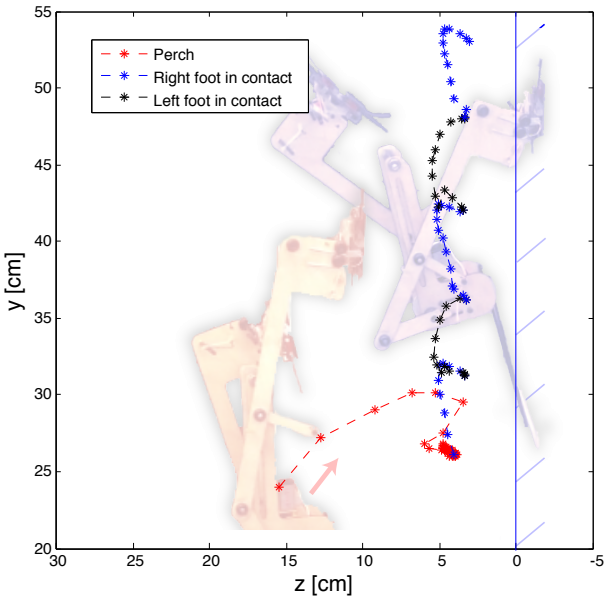

Fig. 8: Center of mass trajectory recorded from video. Red plots the trajectory of a perch at 1.2 m/s $\hat{N}_z$ and 0.6 m/s $\hat{N}_y$ with points plotted at 30 Hz. Blue and black curves plot the trajectory of climbing with points taken at 3 Hz.

limit (i.e. the maximum force that the feet can sustain when loaded at same angle) is plotted in green. The safety factor is the difference between these two curves. Fig. 9 gives a sequence of frames from high speed video recorded during the landings.

Section IV-B discusses the bounds and repeatability of perching with this particular robot while successes and failures in a similar experiment are shown in Fig. 11. A more extensive model and experimental verification of the opposed gripper mechanism can be found in [19].

C. Perch-Crawl Transition

The trajectory of the robot's center of mass during a perch and successive climb is given in Fig. 8. The robot is thrown upright with no angular velocity such that it needs no adjustment in orientation in order to crawl correctly. It is worth noting the irregular motion while climbing, which is a result of compliance in at each ankle joint. Landing robustly in regards to orientation is an ongoing area of work.

IV. Discussion and Design Principles

Insight into the operation of the robot and the design of the gait is provided by the relationships between the forces produced during engagement and detachment. The parameters of the robot are used to construct a simple model to project acceptable landing conditions and compared to recorded successes/failures from force experiments. Finally, the general benefit of compliance within the design is highlighted.

A. Engagement and Detachment Considerations

Interesting cases of the peeling moment, as described in Section II-A, can be seen in the difference in magnitudes

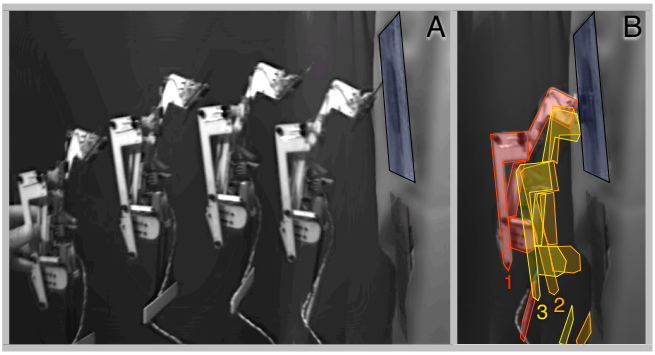

Fig. 9: High speed video shots of perching of the robot showing (A) Trajectory of launch onto outlined, shaded blue glass and (B) Wireframes showing rebound path progressing from red to yellow.

of the normal forces at attachment and detachment. For purposes of highlighting the impact of robot geometry the gravity term is neglected in the analysis, though its contribution is comparable to the considerations presented here.

1) Detachment Forces: The compressive force the incoming foot must exert in order to detach the outgoing foot while climbing upward is affected by the robot's stride length. Once the both feet come into contact, the peeling moment balance is described by (2), using the notation similar to Fig. 4.

$$\begin{aligned}\Sigma\vec{M}^{A/A_{tail}} \cdot \hat{N}_x = \\ (d_{out} + d_{tail})(\vec{F}_{adhesion} \cdot \hat{N}_z) \\ - (d_{in} + d_{tail})(\vec{F}_{compression} \cdot \hat{N}_z)\end{aligned} \quad (2)$$

where d_{out} and d_{in} denote the distance between the bottom of the chassis and the outgoing and incoming feet.

The ratio between the moment arms for the incoming and outgoing feet in the reported experiments is 26:20 cm respectively, or 1.3:1. The magnitude of the engagement force is lower than the detachment force in Fig. 6 as a result of these differing moment arms. A larger stride length allows for lower forces on the incoming foot while detaching a sticky, outgoing foot.

2) Attachment and Tail considerations: Further insight is gained by looking at the peeling moment while the incoming foot is attaching. A long tail length, respective to the stride length, puts less demand on the adhesion required from the anchored foot while a new foot is being attached. Equation 3 gives the relationship between adhesive force required from the anchored foot due to the a compression force necessary to attach an incoming foot.

$$F_{adhesion} = F_{compression}\frac{d_{in} + d_{tail}}{d_{out} + d_{tail}} \quad (3)$$

.

A "safety factor" can be defined as the ratio of adhesion force required to stay attached to the wall (defined by geometry) over the preload force required to engage the incoming foot (fixed by the foot mechanism). Fig. 10 plots this relationship between geometry and safety factor. In this graph, "Tail Length" is considered to be the distance between

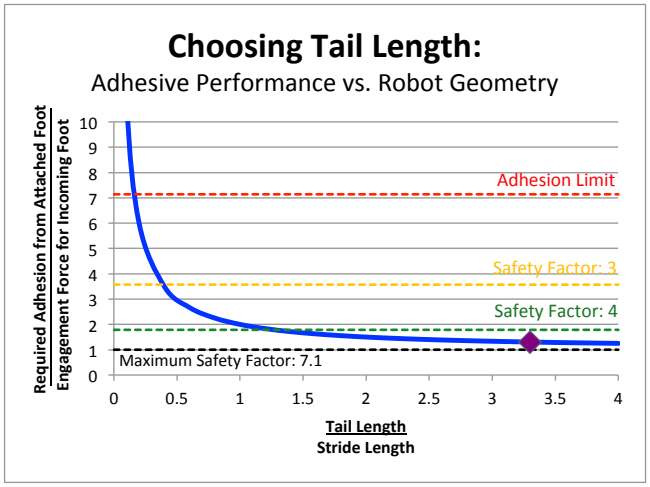

Fig. 10: Curve showing how the choice of stride and tail length affect the required adhesion force for a given preload force necessary to attach incoming foot. For this specific robot, adhesion limit and various safety factors are overlaid (dashed), as well as the point (diamond) representing the chosen geometry indicating its safety factor.

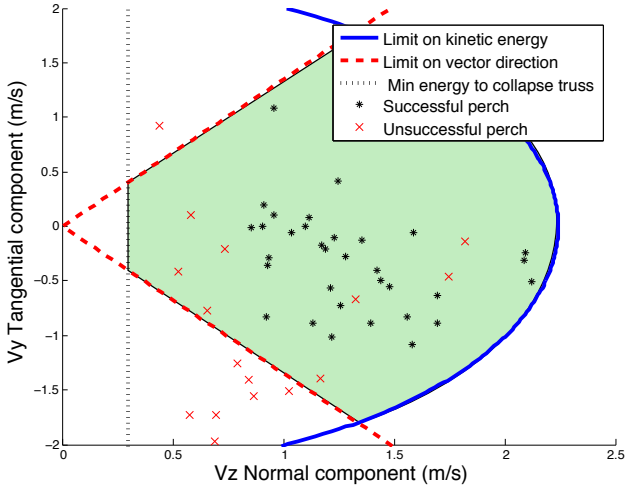

Fig. 11: Bounds on acceptable incoming velocities of the robot for perching with points of recorded successes taken from high speed video. Acceptable conditions are shaded in green.

the lower foot's attachment point and the bottom point of contact at the tail at the wall. Note that the maximum safety factor and minimum ratio of tail length to stride length are set by the adhesive's properties (2.5 N to 0.35 N, or 7.1:1 in this case). The robot presented has a peak safety factor of 5.5 predicted by the moment balance.

B. Bounds on Perching Velocities

Approximate limits on the maximum bounds of suitable conditions for perching are established by considering (1) the ability to dissipate energy, (2) the direction of the incoming velocity vector and (3) the minimum energy needed to collapse the truss.

Assumptions made for these calculations are :

- Negligible angular velocity coming into the wall
- Negligible lateral velocity ($\hat{N}_x$ direction)
- Outriggers successfully align the adhesive to the wall
- Coefficient of restitution of 0.2 is imposed for momentum oriented perpendicular to the wall during impact. The coefficient was empirically determined using in a simple drop test.

The first constraint is a limitation on the trajectory capable of collapsing the truss within the gripping foot, as shown at the bottom of Fig. 3. Jamming will occur if ratio of tangential loading to normal loading in the truss is too large, which puts a constraint on the incoming velocity vector of the foot. The orientation of the vector must be contained within the angle measured between the two truss bars:

$$|2 * \arctan(v_y/v_z)| \leq \theta_{truss} \tag{4}$$

.

The second constraint assumes the maximum energy the robot can absorb during impact is the work stored in the rebound spring. A coefficient of restitution is imposed and potential energy is assume negligible. Thus, the following constraint is imposed to the incoming velocity of the robot:

$$\int F_{Spring}\, dx = 1/2 * m_{robot} * (v_y^2 + 5v_z^2) \tag{5}$$

Lastly, the system must approach the wall with sufficient kinetic energy to collapse the truss. Assuming the maximum force required to collapse the truss (0.35 N) acts throughout its 1 cm travel predicts 0.034 J to collapse the truss.

$$\int F_{Truss}\, dx \leq 1/2 * m_{robot} * (v_z^2) \tag{6}$$

Given these conditions on the maximum ratio between the components in velocity, and the minimum/maximum magnitudes, Fig. 11 shows the bounds on acceptable incoming velocities. Parameters include a truss angle of 105 degrees, an average rebound spring force of 2 N and a travel of 20 cm on the rebound spring. Plotted along with these modeled bounds are empirical points of success and failure recorded from high speed video. Tests were limited to velocities that could be controllably thrown by hand. Results agree generally, but a larger minimum energy appears to be necessary. This is likely due to the force applied at the foot rotating the robot during collision rather than collapsing the truss.

C. Impact Compliance

Compliance is used to manage impact forces, the most notable instance being the foot's rebound spring mitigating forces pulling the feet off the wall. Additionally, compliance in compression during the impact aids in withstanding large, initial tangential forces. Looking at the perching forces in Fig. 7 the highest tangential load can be seen to be approximately 4 N, very close to the maximum adhesion force. However, since the foot is still in compression (i.e. the normal force is still positive), it resists sliding tangentially due to friction with the wall. The ability to prolong the period of compressive force increases the window of time during which the robot can withstand tangential forces and makes landing more tolerant of incoming tangential velocity.

V. Conclusions

A new robotic platform has been demonstrated that achieves both the ability to perch and transition into a climbing gait on a smooth vertical surface. Since both applications provide strong incentive to keep the robot light, the mechanism was built with a minimum of hardware. Enablers of the design were (1) the ability to generate a strong, controllable adhesion and (2) ability to coordinate a cyclic motion of grasping feet through mechanical design.

Design principles illuminated in this robot included managing attachment/detachment forces and the accompanying role of step size and use of a tail. Basic constraints on incoming velocities for successful perching in the absence of angular velocity were outlined: there must be enough energy to collapse the foot's grasping mechanism but not in excess of what can be absorbed by the rebound springs. Additionally, the tangential velocity must be below a certain ratio of the normal velocity. Lastly, compliance between the wall and robot during initial impact was also noted to make the robot more robust to large, tangential forces.

VI. Future Work

Future work includes further improvement of several functional aspects of the robot. The current design, which was constrained by modularity and need for disassembly during development, could be made lighter and stronger, allowing higher collision speeds and/or smaller adhesive pads.

Additionally, the detachment force of the adhesive is higher than necessary. Directional adhesives with a lower pull-off pressure [16] are possible and would be preferable.

Furthering the capabilities of the robot, modification of the crawling gait and feet attachment would allow the robot to adhere to inverted surfaces.

Dynamic control of the platform offers an opportunity to explore desirable landing conditions. Use of an active inertial or drag-inducing tail to control orientation and/or pitch rate could increase chances of a successful landing.

Acknowledgments

We thank Nick Kohut, Morgan Pope, Hao Jiang and other members of the Biomimetic and Dexterous Manipulation Lab for the advice and support throughout the project. Support was provided by NSF IIS-1161679 and ARL MAST MCE 14-4. Matt Estrada is additionally supported by the NSF Graduate Research Fellowship. Elliot Hawkes is supported by the NSF Graduate Research Fellowship and (NDSEG) Fellowship.

References

[1] J. Lecoeur, L. Daler, P. B. Hählen, D. Floreano *et al.*, "A flying robot with adaptive morphology for multi-modal locomotion," in *Intelligent Robots and Systems (IROS), 2013 IEEE/RSJ International Conference on*, no. EPFL-CONF-187750, 2013.

[2] A. Kalantari and M. Spenko, "Design and experimental validation of hytaq, a hybrid terrestrial and aerial quadrotor," in *Robotics and Automation, 2013. Proceedings. ICRA'13. IEEE International Conference on*, 2013.

[3] K. Peterson and R. S. Fearing, "Experimental dynamics of wing assisted running for a bipedal ornithopter," in *Intelligent Robots and Systems (IROS), 2011 IEEE/RSJ International Conference on*. IEEE, 2011, pp. 5080–5086.

[4] J. D. Dickson and J. E. Clark, "Design of a multimodal climbing and gliding robotic platform," *Mechatronics, IEEE/ASME Transactions on*, vol. 18, no. 2, pp. 494–505, 2013.

[5] D. F. Hougen, S. Benjaafar, J. C. Bonney, J. R. Budenske, M. Dvorak, M. Gini, H. French, D. G. Krantz, P. Y. Li, F. Malver *et al.*, "A miniature robotic system for reconnaissance and surveillance," in *Robotics and Automation, 2000. Proceedings. ICRA'00. IEEE International Conference on*, vol. 1. IEEE, 2000, pp. 501–507.

[6] L. Daler, A. Klaptocz, A. Briod, M. Sitti, and D. Floreano, "A perching mechanism for flying robots using a fibre-based adhesive," in *Robotics and Automation (ICRA), 2013 IEEE International Conference on*. IEEE, 2013, pp. 4433–4438.

[7] E. W. Hawkes, D. L. Christensen, E. V. Eason, M. A. Estrada, M. Heverly, E. Hilgemann, H. Jiang, M. T. Pope, A. Parness, and M. R. Cutkosky, "Dynamic surface grasping with directional adhesion," in *Intelligent Robots and Systems (IROS), 2013 IEEE/RSJ International Conference on*. IEEE, 2013, pp. 5487–5493.

[8] A. L. Desbiens, A. T. Asbeck, and M. R. Cutkosky, "Landing, perching and taking off from vertical surfaces," *The International Journal of Robotics Research*, vol. 30, no. 3, pp. 355–370, 2011.

[9] C. E. Doyle, J. J. Bird, T. A. Isom, J. C. Kallman, D. F. Bareiss, D. J. Dunlop, R. J. King, J. J. Abbott, and M. A. Minor, "An avian-inspired passive mechanism for quadrotor perching," *Mechatronics, IEEE/ASME Transactions on*, vol. 18, no. 2, pp. 506–517, 2013.

[10] M. Spenko, G. C. Haynes, J. Saunders, M. R. Cutkosky, A. A. Rizzi, R. J. Full, and D. E. Koditschek, "Biologically inspired climbing with a hexapedal robot," *Journal of Field Robotics*, vol. 25, no. 4-5, pp. 223–242, 2008.

[11] J. Dickson and J. Clark, "The effect of sprawl angle and wall inclination on a bipedal dynamic climbing platform," in *Proc. 15th Int. Conf. Climbing Walking Robots Support Technology*, 2012.

[12] S. Kim, M. Spenko, S. Trujillo, B. Heyneman, D. Santos, and M. R. Cutkosky, "Smooth vertical surface climbing with directional adhesion," *Robotics, IEEE Transactions on*, vol. 24, no. 1, pp. 65–74, 2008.

[13] M. P. Murphy and M. Sitti, "Waalbot: An agile small-scale wall-climbing robot utilizing dry elastomer adhesives," *Mechatronics, IEEE/ASME Transactions on*, vol. 12, no. 3, pp. 330–338, 2007.

[14] M. P. Murphy, C. Kute, Y. Mengüç, and M. Sitti, "Waalbot ii: Adhesion recovery and improved performance of a climbing robot using fibrillar adhesives," *The International Journal of Robotics Research*, vol. 30, no. 1, pp. 118–133, 2011.

[15] P. Birkmeyer, A. G. Gillies, and R. S. Fearing, "Dynamic climbing of near-vertical smooth surfaces," in *Intelligent Robots and Systems (IROS), 2012 IEEE/RSJ International Conference on*. IEEE, 2012, pp. 286–292.

[16] P. Day, E. V. Eason, N. Esparza, D. Christensen, and M. Cutkosky, "Microwedge machining for the manufacture of directional dry adhesives," *Journal of Micro and Nano-Manufacturing*, vol. 1, no. 1, p. 011001, 2013.

[17] D. I. Goldman, T. S. Chen, D. M. Dudek, and R. J. Full, "Dynamics of rapid vertical climbing in cockroaches reveals a template," *Journal of Experimental Biology*, vol. 209, no. 15, pp. 2990–3000, 2006.

[18] D. Santos, M. Spenko, A. Parness, S. Kim, and M. Cutkosky, "Directional adhesion for climbing: theoretical and practical considerations," *Journal of Adhesion Science and Technology*, vol. 21, no. 12-13, pp. 1317–1341, 2007.

[19] H. Jiang, M. Pope, E. W. Hawkes, D. Christensen, M. Estrada, A. Parlier, R. Tran, and M. Cutkosky, "Modeling the dynamics of perching with opposed-grip mechanisms," in *Robotics and Automation, 2014. Proceedings. ICRA'14. IEEE International Conference on*, 2014.